Mapping the health benefits of greenspace against urban heat exposure through an ecosystem services framework

Abstract

We provide a novel method to assess the heat mitigation impacts of greenspace though studying the mechanisms of ecosystems responsible for benefits and connecting them to heat exposure metrics. We demonstrate how the ecosystem services framework can be integrated into current practices of environmental health research using supply/demand state-of-the-art methods of ecological modeling of urban greenspace. We compared the supply of cooling ecosystem services in Boston measured through an indicator of high resolution evapotranspiration modeling, with the demand for benefits from cooling measured as a heat exposure risk score based on exposure, hazard and population character- istics. The resulting evapotranspiration indicator follows a pattern similar to conventional greenspace indicators based on vegetation abundance, except in warmer areas such as those with higher levels of impervious surface. We identified demand-supply mismatch areas across the city of Boston, some coinciding with affordable housing complexes and long term care facilities. This novel ES-framework provides cross-disciplinary methods to prioritize urban areas where greenspace interventions can have the most impact based on heat-related demand.

GRAPHICAL ABSTRACT

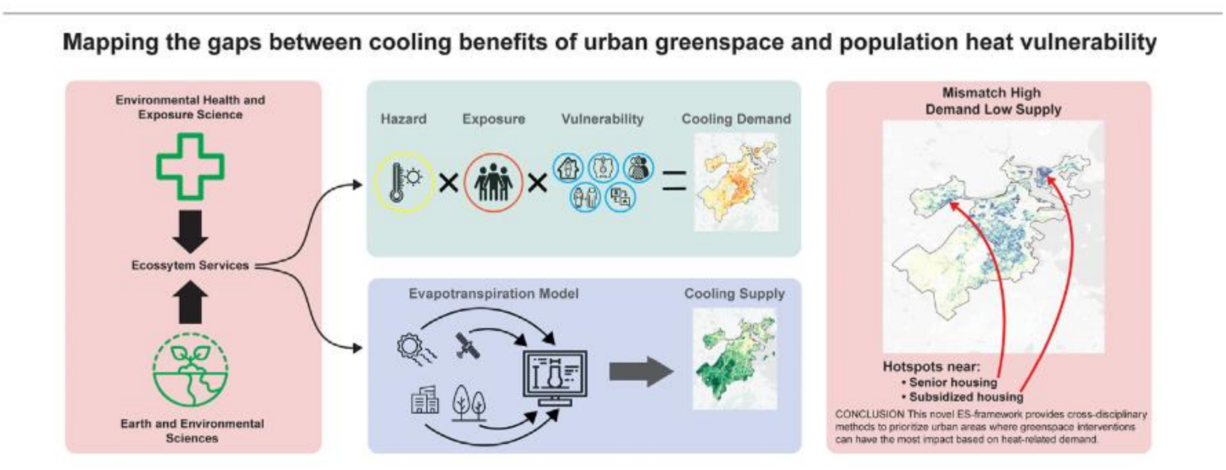

Tiesken, K., Smith, I.A., Jimenez Celsi, J.B., Hutyra, L.R., Fabian, M.P. Mapping the Cooling Health Benefits of Greenspace through an Ecosystem Services Framework. Science of the Total Environment, 845(1): 157283, 2022.

1. Introduction

Evidence shows that exposure to urban greenspace is associated with a wide array of health benefits including reduced cardiovascular disease, improved mental health, and reduced mortality (Twohig-Bennett and Jones, 2018; van den Berg et al., 2015). Various pathways have been identified for this association, such as the capacity of vegetation to regulate temperature, improve air quality, provide opportunity for physical activity, and reduce mental stress (James et al., 2015). Despite the variety in pathways, greenspace exposure is often operationalized with a metric of vegetation abundance derived from satellite imagery such as the Normalized Vegetation Index (NDVI), or the location of certain types of greenspace (e.g. distance to parks of public gardens) from detailed land use data.

While current NDVI products are among the most accurate and spatially resolved data at the disposal of the epidemiologist, their application as exposure metric can lead to overlooking the intricate ties between ecosystems and their physical and social environments that moderate or mediate health effects. For instance, Leslie et al. (2010) showed that mental health outcomes were more associated with one’s perception of available greenspace than with measures of vegetation abundance. Relying on metrics of vegetation abundance or proximity has prevented methods to empirically separate different pathways and answer *how* greenspace exposure improves our health (Shanahan et al., 2015). To better understand if, where, and why greenspace exposure affects health outcomes there is a need for a holistic framework that can connect health benefits with ecosystem functions and mechanisms relying on literature from both health and ecological sciences (Zhang et al., 2017).

To distinguish different health effects of greenspace, reduce exposure misclassification, and provide a more causal narrative of health effects of greenspace, several authors have suggested adopting a framework of ecosystem services (ES), focusing on vegetation activity relevant to health outcomes (Bratman et al., 2019; Chiabai et al., 2018; Frumkin et al., 2017; Sandifer et al., 2015; Shanahan et al., 2015). ESs can be defined as “the aspects of ecosystems utilized (actively or passively) to produce human well-being” (Fisher et al., 2008), and are valued based on the benefits they produce for humans. Through a focus on quantitatively linking human benefits with functions of the natural environment, the ES-framework can be seen as a set of definitions and tools that forms a bridge between fields to promote inter-disciplinary research on the value of nature (Phillipson et al., 2009). This interdisciplinary approach facilitates incorporating knowledge about ecological mechanisms such as particulate matter deposition and air filtration (Janhäll, 2015) or ambient cooling (Winbourne et al., 2020; Yunusa et al., 2015) into the domain of health sciences.

In this paper we demonstrate how the ES-framework can be used to integrate state-of-the-art methods of ecological modeling into current practices of environmental health research focusing on ambient cooling capacities of urban greenspace and linking it to risk of residential exposure to extreme heat. Exposure to extreme heat is associated with various health outcomes including increased mortality (Medina-Ramón and Schwartz, 2007), higher numbers of emergency department-visits (Hess et al., 2014), and adverse pregnancy outcomes (Bekkar et al., 2020). Heat exposure risk is exacerbated in urban environments where impervious surfaces such as concrete and asphalt absorb solar radiation causing higher temperatures in urban centers than in surrounding rural areas (Kleerekoper et al., 2012). Urban greenspace can reduce the this urban heat island (UHI) effect through shading and evapotranspiration (Winbourne et al., 2020; Yan et al., 2020).

Recently, various research groups have developed various tools and instruments to assess the capacity of urban greenspace to mitigate urban heat through evapotranspiration and shading. Most notably the InVEST Urban Cooling Model, developed by the Natural Capital Project includes a land cover based urban cooling model to estimate the urban cooling capacity of greenspace (Zardo et al., 2017). As one of the strengths of this model lies in its global applicability, a local model can provide improvement in terms of modeling the complex interaction between climatological conditions, radiation, and evapotranspiration (Zawadzka et al., 2021). In previous work we developed one of the first high resolution spatially explicit models of urban evapotranspiration (Smith et al., 2021). By comparing spatially modeled levels of evapotranspiration with a risk assessment of extreme heat exposure, we test to what extent temperature regulating ecosystem service provides benefits in terms of human health gains. In doing so we provide one of the first attempt to apply ecosystem services assessments in environmental health research.

2. Methods

2.1.1. Overview

We used an ES-approach by comparing the supply of cooling ecosystem services to the demand for health benefits from cooling in Boston, MA. We mapped the supply of temperature regulating ES by modeling the level of evapotranspiration during a local heatwave at a 30m scale of the current vegetation cover of Boston (Smith et al., 2021). While vegetation provides cooling benefits through both shading and evapotranspiration, this analysis focuses on the evapotranspiration mechanism as the daytime urban heat island intensity is primarily driven by variations in the capacity of urban and rural areas to evaporate water (Li et al., 2019). Thus, cooling via evapotranspiration represents a key ES to city residents and spatially co-occurs with shading benefits as well. We estimated the demand for health benefits from heat reduction as a spatial risk assessment of extreme heat exposure multiplying spatial layers of exposure, hazard, and heat vulnerability (Aubrecht and Özceylan, 2013; Tomlinson et al., 2011). We chose to model exposure to extreme heat as we expect the greatest local variation and therefore the highest spatial heterogeneity of potential for health benefits.

2.1.2. Location

Boston is a city located in the Northeast of the United States and has an estimated population size of almost 692,600 people in 2019. Boston has a continental climate of relatively cold winters and hot and humid summers, with average maximum daily temperatures in July of 27^{o}C and an average of 15 days per year of ambient temperatures above 30^{o}C.

2.2. Cooling Demand through Heat Risk Exposure Index

We operationalized the demand for cooling using the following heat risk index equation based on a study by Aubrecht et al. (2013):

$$HRI = HVI_i * \ P(hwday)_i * \ POP_i$$

where heat risk exposure index (HRI) at 30 m pixel *i* is calculated by the probability for local heat wave day conditions (P(hwday)) multiplied by the heat vulnerability index (HVI) multiplied by the population (POP) to account for the level of exposure at pixel *i*. Equation terms are further detailed below. Pixel resolution was 30m in order to get a fine-scaled distribution of heat risk that can be compared with supply model outputs.

2.2.1. Probability for local heat wave day conditions (P(hwday))

Extreme heat exposure was assigned by calculating the probability of a local (30 m) heat wave, given evidence that heatwaves impact health more than single days of extreme temperatures (Kent et al., 2014; Madrigano et al., 2015). For spatially explicit ambient temperatures we used PRISM climate data, which consist of daily minimum and maximum temperatures for the United States modeled at 800m resolution using a range of biophysical land characteristics and air temperatures from monitoring stations (PRISM Climate Group, 2019). Daily maximum ambient temperatures at a 30m resolution were calculated by downscaling 800m PRISM maximum daytime temperature data with 30m impervious surface area (ISA) (MassGIS 2019) and time of year based on previously observed relationships where for every day of the year a regression coefficient was provided for ISA's effect on ambient temperature

(Wang et al., 2017). Since ISA was not used in the PRISM model, we used a 30m dataset of ISA adjust local temperatures based on ISA. The downscaled temperature (T) at 30m pixel I on the j^{th} day was calculated as:

$$T_{i,j} = T_{prism,i,j} + \beta_j \, ISA_i$$

where T_{prism} is the 800m PRISM maximum temperature that corresponds with pixel i on day j, β is a mean-centered coefficient reflecting the effect of impervious surface on ambient temperature for the corresponding month of day j (Wang et al., 2017) and ISA is the impervious surface area at pixel i. The result was a grid of maximum daily ambient temperature at 30 m resolution for June, July and August.

We defined a local heatwave as two consecutive days of maximum daytime temperatures above the 95^{th} percentile in Boston during the months of June, July, and August (Spangler and Wellenius, 2020). To calculate the probability of a heatwave day at a specific pixel we divided the number of times two consecutive days the maximum temperature was above the 95^{th} percentile by the total number of summer days during the months of June, July, and August between the years of 2008 and 2018. Final calculations resulted in values that could theoretically be between 0 and 1 for each 30 meter pixel, representing the probability for a local heat wave conditions on a given day in the summer months.

2.2.2. Heat vulnerability Index (HVI)

We built a heat vulnerability index composed from demographic and socio-economic factors that are correlated with higher heat-related hospitalizations and mortality (Madrigano et al., 2018; Reid et al., 2009; Riley, 2018; Spangler and Wellenius, 2020). We included five dimensions of heat vulnerability at the census block group level using data from the American Community Survey (ACS) (5-year estimates 2013-2018): 1) age (percentage of people over 65 years); 2) poverty (percentage of people with income below poverty line minus percentage of people enrolled in higher education to account for students (Bishaw, 2013)); 3) language-barriers (percentage of people speaking English less than well); 4) vulnerable living situation (percentage of people older than 65 living alone); and 5) racial minority composition (percentage of non-white people). We summed the percentages of population of each variable in census block group in Boston and divided the final score by the highest total value to calculate a heat vulnerability index ranging from 0 to 1 (Aubrecht and Özceylan, 2013). In absence of empirical evidence relating these dimensions to health outcomes in Boston, we assumed all five dimensions had the same relative importance.

2.2.3. Population (Pop)

To estimate the number of people living at each 30m pixel in Boston, we downscaled the Census 2010 population counts by census block to population in buildings by distributing the total count of population per census block over the surface area of residential buildings (Xie, 2006). We used Open Street Map (OpenStreetMap, 2017) to identify all buildings in Boston and filtered out non-residential buildings using parcel level tax data from the Massachusetts Tax Assessor (MassGIS, 2020) and the City of Boston (Boston Assessing Department, 2019). Population per 30m pixel was calculated as the census block population multiplied by the proportion of residential building surface area compared to the total surface area of each census block. We used Census 2010 count data to minimize error within a census unit, since ACS data are not available at the census block level. The population data was log transformed to normalize the distribution.

The Heat Risk Index (HRI) was calculated by multiplying *(P(hwday))*HVI*POP* and the final demand map was generated by smoothing the HRI of the neighborhood within a radius of 60m from each 30m pixel to match the radius of cooling ES of evapotranspiration described below.

2.3. Cooling Supply from Greenspace: Latent Heat Flux

We developed a remote sensing driven evapotranspiration model (Smith et al., 2021) based on a Penman-Monteith formulation that couples a carbon light-use efficiency model, Geostationary Operational Environmental Satellite-16 (GOES-16) radiation (NOAA National Centers for Environmental Information, 2017), Rapid Refresh (RAP) temperature analysis data (Benjamin et al., 2016), impervious surface maps (MassGIS, 2007), Landsat albedo (Trlica et al., 2017) and Landsat enhanced vegetation index (EVI) (Retrieved from Google Earth Engine; Gorelick et al., 2017). Evapotranspiration, measured as latent heat flux (λE; W m^{-2}) was modeled for the City of Boston, MA at hourly time steps and a spatial resolution of 30 meters during a 6-day heatwave event from August 2 – August 7, 2018 where the mean air temperature across the modeling domain was 28.7°C, approximately 25% warmer than the mean 2018 6-day rolling average temperature during June, July, and August (23.0°C).

Full description of the evapotranspiration model can be found in Smith et al., (2021). Briefly, the modeling approach consisted of three core equations to estimate latent heat flux contributions from vegetation and did not consider other sources of urban latent heat flux, such as evaporation from lakes or standing water. Vegetation activity was characterized as a function of incoming solar radiation via estimates of net canopy photosynthesis (defined as the difference between the gross ecosystem exchange of CO_2 and canopy respiration of CO_2) produced using the Urban Vegetation Photosynthesis and Respiration Model (Hardiman et al., 2017; Mahadevan et al., 2008) as:

$$A_n = \left(\delta \cdot T_{scale} \cdot P_{scale} \cdot W_{scale} \cdot EVI \cdot \frac{1}{1+ {PAR}/{PAR_0}} \cdot PAR\right) - 0.1 \cdot R_{eco}$$

where A_n is net photosynthesis (net assimilation of CO_2; µmol CO_2 m^{-2} s^{-1}), δ is a plant functional type-specific light-use efficiency (µmol CO_2 µmol PAR^{-1}), T_{scale}, P_{scale}, and W_{scale} are dimensionless scaling terms ranging from zero to one describing the influence of air temperature, phenology, and moisture on photosynthesis, *EVI* is the enhanced vegetation index, *PAR* is incoming photosynthetically active radiation (µmol m^{-2} s^{-1}), PAR_0 is the plant functional type-specific optimized half-saturation value (µmol m^2 s^{-1}), and R_{eco} is ecosystem respiration (µmol CO_2 m^2 s^{-1}). Temperate deciduous broadleaf plant functional type parameters from Mahadevan et al. (2008) were applied to characterize vegetation in Boston, MA, consistent with local vegetation surveys (Urban Ecology Institute, 2008). Leaf level respiration is assumed to be 10% of ecosystem respiration (Tang et al., 2008). Air temperature data was adjusted as a function of impervious surface area following the methods described in Wang et al. (2017) and Hardiman et al. (2017).

The net photosynthesis estimates from the VPRM are used to estimate stomatal (or surface) conductance, the process governing the land surface's ability to evaporate water, via the Medlyn et al. (2011) stomatal conductance model as:

$$g_s = g_0 + 1.6 \cdot \left(1 + \frac{g_1}{\sqrt{D}}\right) \cdot \frac{A_n}{{c_s}/{P_{atm}}}$$

where g_s is the stomatal conductance (µmol H_2O m^{-2} s^{-1}), g_0 is the minimum value of stomatal conductance (100 µmol H_2O m^{-2} s^{-1}), g_1 is a plant functional type-specific parameter, D is the vapor pressure deficit (kPa), A_n is the net assimilation of CO_2 (µmol CO_2 m^{-2} s^{-1}), c_s is the atmospheric partial pressure of CO_2 (40.53 Pa), and P_{atm} is the atmospheric pressure (101,325 Pa).

Given estimates of surface conductance, latent heat flux is estimated using the Penman-Montieth equation of evapotranspiration (Monteith, 1965) as:

$$\lambda E = \frac{\Delta(R_n - G) + \rho_a c_p (D) g_a}{\Delta + \gamma(1 + {g_a}/{g_s})}$$

where λ is the latent heat of vaporization of H_2O (2260 J g^{-1}), E is the mass H_2O evaporation rate (g s^{-1} m^{-2}), Δ describes the rate of change of saturation specific humidity with air temperature (Pa K^{-1}), R_n is the net radiation balance of the surface (W m^{-2}), G is the ground heat flux (W m^{-2}), ρ_a is the dry air density (1.275 kg m^{-3}), c_p is the specific heat capacity of air (1005 J kg^{-1} K^{-1}), D is the vapor pressure deficit (Pa), g_a is the atmospheric conductance (m s^{-1}), g_s is the surface conductance (m s^{-1}), and γ is the psychrometric constant (66 Pa K^{-1}). A more detailed description of equation terms and sources is provided in the SI. Latent heat flux estimates were averaged within a radius of 60m for every 30-m pixel to reflect the typical spatial scale of vegetation induced cooling in cities (Ziter et al., 2019).

Previous research showed that transpiration levels of vegetation are positively correlated with ambient temperature, meaning that especially during heat waves evapotranspiration may be higher in more urbanized areas (Winbourne et al., 2020). To assess how this indicator differs from traditional vegetation abundance indicators we calculated a bivariate correlation between EVI at 30m resolution and latent heat flux during heat wave conditions at similar resolution.

2.4. Demand supply comparison

A mismatch between low supply and high demand for an ecosystem service indicates a potential for relatively high benefits from additional increase in ecosystem service supply (Burkhard et al., 2012). High cooling demand (high heat exposure risk index) and low cooling supply (low levels of latent heat flux) areas were identified by transforming supply and demand to percentile rank (PR) scores to reduce bias (Schulp et al., 2014). PR scores were calculated excluding pixels where HRI = 0. We multiplied the PR of demand with the inverted PR (100 - PR) of supply and divided it by the maximum possible score (99^2) to generate a map of the share of instances each pixel was designated high demand–low supply out of the 9,801 (99^2) possible combinations of percentile thresholds as done previously in Tieskens et al. (2017). A value close to 1 indicates a mismatch regardless of a threshold distinguishing between high and low supply and demand.

Additionally, we ran a linear regression model to assess which aspects of the ES demand were related to the ES-supply. The linear model predicted the ES-supply as latent heat flux per census block group in Boston with the five HVI variables, the average heatwave probability, and the total population. To calculate average heat wave probability and latent heat flux per census block group we masked the area of each census block group with the building footprint of residential buildings to only include supply and demand variables at locations of residential heat exposure. To account for multi-collinearity we calculated variation inflation factors (VIF) for each predictor using the CAR package in R software (Fox, John & Weisberg, 2011). As no VIF was higher than 3 we did not exclude any predictor from the model.

3. Results

3.1. Cooling Demand through Heat Risk Exposure Index

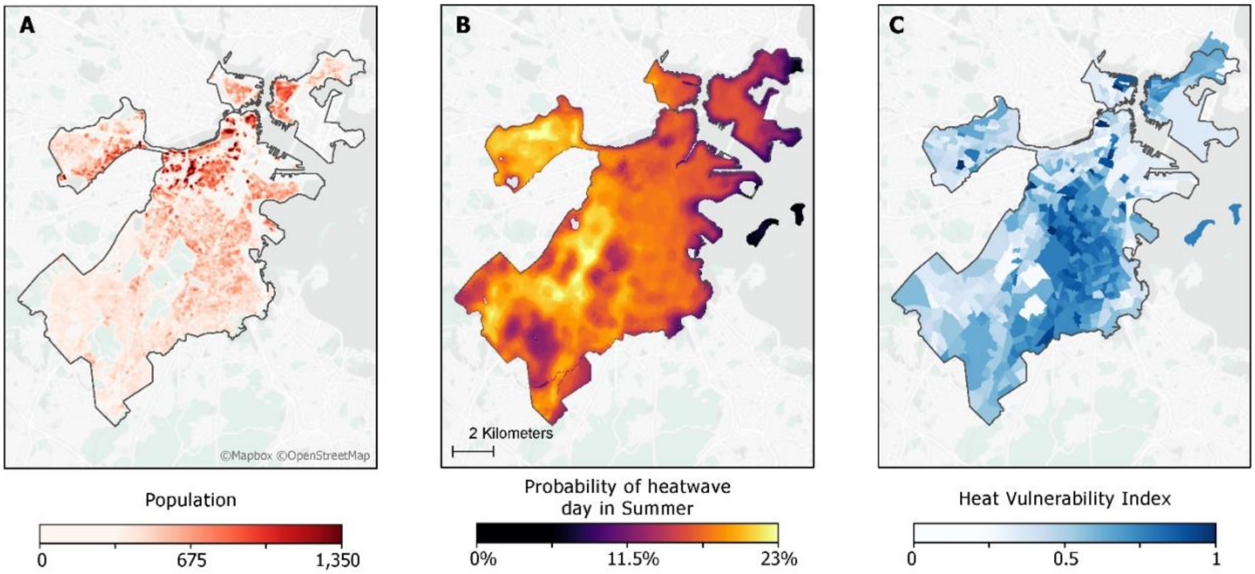

Figure 1 Map of Boston showing: A: Total population at 30m resolution; B: Probability of a summer heatwave day at 30 meter resolution; C: Sociodemographic heat vulnerability index at a block group level

Figure 1 shows the spatial distribution of the three components of the heat risk index (i.e. cooling demand): population, heatwave probability, and heat vulnerability index. The probability of a local heat wave day ranged between 0 and 23%, with the highest values close to the center of Boston (Figure 1B, light yellow areas). Areas with lower probabilities (dark shades in Figure 1B) are found on the harbor islands, coast and in the southwest of the city, which coincides with locations of parks and urban forests. The heat vulnerability index map (Figure 1C) shows a stark differences between neighborhoods. The highest values were found in inner city neighborhoods of Boston, characterized by high percentages of people living below the poverty line and high percentages of racial minorities. In the northwest of the city isolated hotspots were mostly driven by the percentage of people over 65 years living alone.

Figure 2A shows the results of the integrated heat exposure risk index map (Figure 2A), showing a clear difference between the south west side of Boston characterized by a relatively low cooling demand with values close to 0 while high demand is concentrated in the north east side of the city, and the centrally located inner cities with values between 0.6 and 1. There are several areas in the city with concentrated pockets of very high demand surrounded by lower demand.

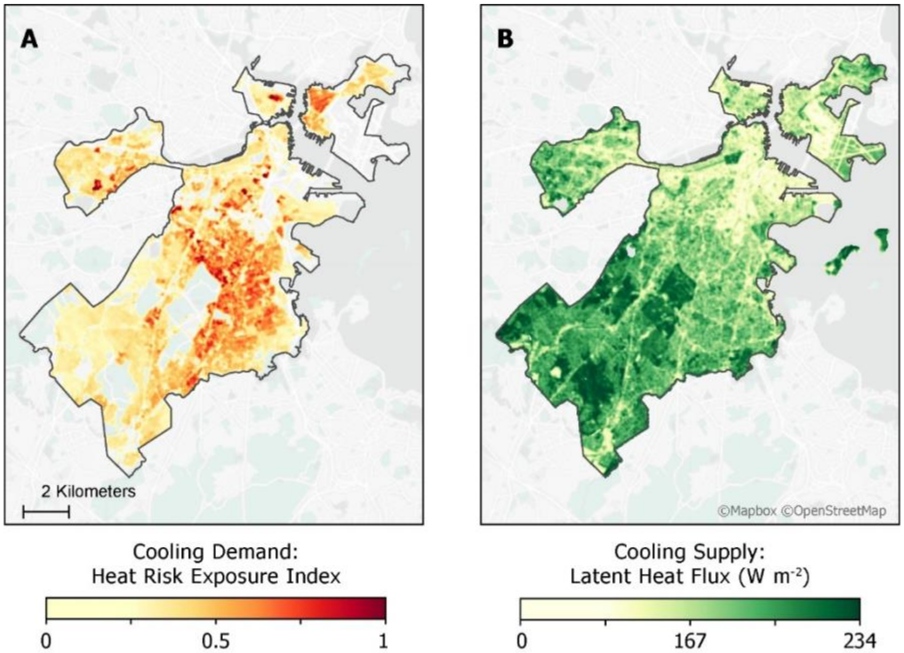

Figure 2 Map of Boston at 30 m resolution showing: A) Demand for cooling as heat risk exposure index, and B) Greenspace cooling supply as Latent Heat Flux

3.2. Cooling Supply from Greenspace: Latent Heat Flux

Figure 2B shows an example of the spatial distribution of the cooling supply from greenspace across Boston on a heatwave day at noon. The average supply of greenspace cooling via transpiration was 85.6 W m^{-2} across the city during the modeling period. We observed substantial spatial heterogeneity in the magnitude of latent heat fluxes with maximum latent heat flux rates found in the more heavily vegetated areas of the city and minimum rates found in the portions of the city with the most impervious surface area (Figure 2B), ranging from 0 – 334.5 W m^{-2}. A bivariate correlation analysis showed a high correlation between latent heat flux and EVI ($r=0.99$, $p <0.001$). However, we found a range of latent heat flux estimates for pixels with similar EVI that varied as a function of urbanization as pixels with higher fractions of ISA tend to have warmer temperatures and higher vapor pressure deficits in the atmosphere, ultimately driving increases in transpiration rates.

The plot in figure 3 shows that the correlation between latent heat flux and EVI is not completely linear as for both tails of the EVI distribution latent heat flux is lower than predicted by EVI only.

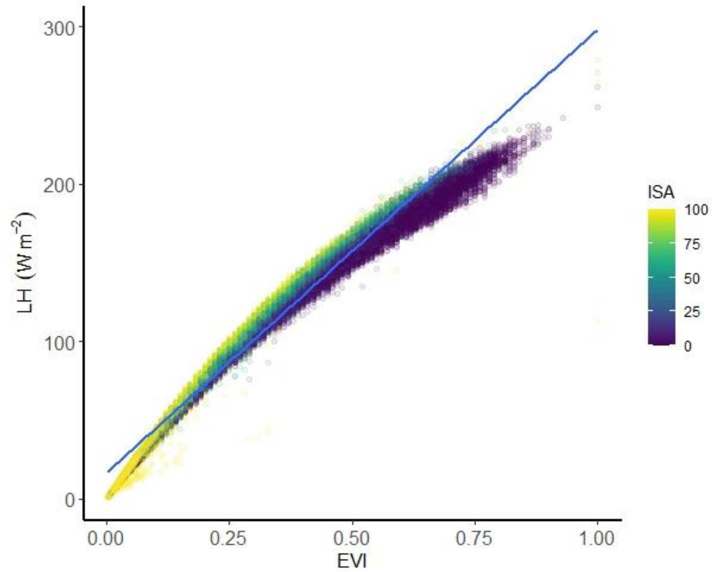

3.3. Demand supply comparison

Figure 5A shows the high/low cooling supply/demand comparison across Boston. Areas shaded with a value between 0.8 and 1 in dark blue have an estimated mismatch of demand and supply in at least 80% of all possible combination of percentile rank definitions of high demand and low supply. Similar to the demand distribution (Figure 2A) the comparison shows high values in the inner cities and concentrated hotspots around Boston. We zoomed in to three different areas in the city to highlight notable differences and patterns. We found some of the highest concentration for demand for health benefits of cooling in Brighton, a community home to some of the housing complexes in the city housing older adults, often living alone. Figure 4B-1 shows that the high demand coincides with the location of these complexes. Figure 4B-2 shows that this area is also characterized by a relatively high cooling ES supply, reducing the value of the comparison index in Figure 4A. Figure 4C shows a similarly concentrated pattern of demand in Chinatown, not driven by high population counts of elderly, but instead by high population density and a relatively large share of low income families not identifying as white. Here, high concentrations of demand coincide with the location of several large affordable housing complexes. Despite the relative proximity of these complexes there is a significant difference in ES supply. Figure 4C-2 shows that the supply of cooling was low around the two most eastern complexes while the being higher around the south western complex. The most striking hotspot of ES mismatch appeared in East Boston (Figure 4D). Despite two affordable housing complexes the high level of demand was spread over the entire neighborhood. This neighborhood is home to a large community of people identifying as Hispanic/Latino, with relatively high numbers of non-English speakers. Figure 4D-2 shows that the high demand was met with low levels of evapotranspiration throughout the neighborhood.

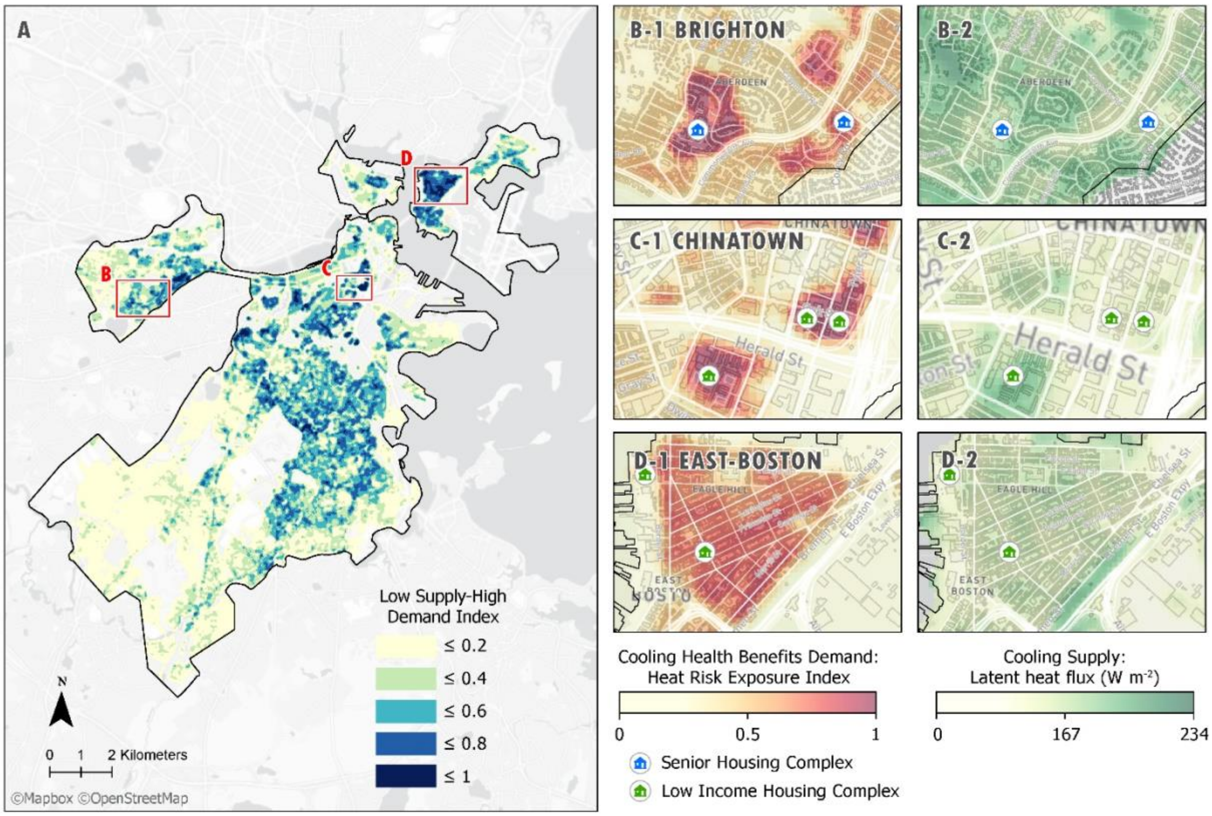

Figure 4 A: Frequency index of low supply-high demand designation for each combination (99^2) of percentile definition of low-supply and high-demand. B 1– D 1: zoom in maps showing Cooling Health Benefits Demand. B 2 – D 2: Zoom in maps showing Cooling Supply

A linear model explaining the latent heat flux per census block group with the variables that composed the ES-demand function shows that the percentage of people older 65, the percentage non-white population and the probability for a heatwave were positively correlated with the ES-supply.

Table 1 Regression coefficients of ordinary least squares linear model explaining latent heat flux with dimensions of heat vulnerability, heat hazard, and exposure (population).

	Estimate	Std. Error	P-value
Intercept	-1.78	10.67	0.87
Percentage living below poverty line	-17.95	9.61	0.06
Percentage older than 65	131.09	15.38	< 0.001
Percentage older than 65 and living alone	-129.17	29.96	< 0.001
Percentage speaking English less than well	-59.98	11.35	< 0.001
Percentage non-white population	27.09	4.11	< 0.001
Heat wave probability	420.91	57.07	< 0.001
Population	0.00	0.00	0.36

Adjusted $R^2 = 0.28$

The percentage of people living below the poverty line, the percentage of people being older than 65 and living alone, and the percentage of people speaking English less than well was negatively correlated with ES-supply. The total number of people living in each census block group was not significantly correlated with the supply of cooling ecosystem services.

4. Discussion

With this paper we attempted to use the ecosystem services framework to improve understanding of the health effects of urban greenspace, focusing on heat mitigation. By spatially comparing cooling ES supply with heat exposure risk, serving as a proxy for demand for health benefits of cooling, we revealed those areas within the city where additional urban vegetation could provide the highest benefits in terms of heat related health outcomes. Modeled evapotranspiration as an indicator of greenspace activity showed a very similar pattern to conventional indicators based on vegetation abundance. However, we revealed a pattern of stronger cooling potential per tree in more urban areas with higher impervious surface fractions. Zooming in on several demand-supply mismatch hotspots revealed that strong concentrations coincided with affordable housing complexes or housing for older adults.

While our study identified areas where supply did not meet the demand for urban cooling, we also showed that on average the supply of cooling ES was positively correlated with heat hazard and several dimensions of our HVI including old age and non-white populations. This is an interesting finding as recent studies exposed systemic racial inequities in terms of greenspace exposure in US cities revealing a striking pattern of consistently lower levels of vegetation in neighborhoods with that suffered from racially discriminatory zoning practices and higher shares of people of color (Nardone et al., 2021). The reason for the different finding could be that we only accounted for ES-supply of residential cooling and did not include any vegetation that was not located within 60m of a residential building.

At first sight, the comparison between the proposed indicator of cooling ES services and the common indicator of EVI may indicate that the potential for exposure misclassification associated with vegetation abundance indicators is limited (Cf. Nouri et al., 2014). However, we revealed a pattern of stronger cooling potential per tree in more urban areas with higher impervious surface fractions. This finding suggests that previous studies that linked reduced heat mortality to greenspace exposure based on indicators of greenspace abundance (Burkart et al., 2016; Gronlund et al., 2015; Madrigano et al., 2015; Tan et al., 2007) might have underestimated the cooling effect of greenspace in inner cities with higher impervious surface area inducing higher local temperatures and by extension higher evapotranspiration. Inner cities not only report the highest peak temperatures during heatwaves, but often also house a disadvantaged population of low income minority households suffering from structural racism and social isolation (Rankin and Quane, 2000; Watson and Wilson, 1988) associated with higher vulnerability to extreme heat exposure (Aubrecht and Özceylan, 2013; Gronlund et al., 2015; Reid et al., 2009).

The effect of greenspace on heat related health outcomes has been recognized and analyzed in many previous studies (see Markevych et al., 2017; Tomlinson et al., 2011; Twohig-Bennett and Jones, 2018). Likewise, the effect of vegetation on urban temperatures has been the topic of many ecological and environmental studies (Adams and Smith, 2014; Gallo et al., 1993; Hu and Li, 2020). Yet, the connection between these two fields has been limited. We used the ES-framework to connect the work done in these two broad fields. The heat risk index can be a starting point for ecosystem services mapping studies to incorporate public health methods for more accurate operationalization of health benefits. The heat vulnerability index proposed in this paper could, for instance, be a great addition to the widely used InVEST urban cooling model that currently relies on a linear relationship between temperature and mortality to estimate potential health benefits from urban cooling (Hamel et al., 2021). Moreover, the explicitly urban evapotranspiration modeling presented here (and further explained in Smith et al. (2021)) is one of the first mechanistic evapotranspiration models explicitly designed for urban context and can provide hourly outputs. This mechanistic model can be used to improve current cooling models such as the InVEST Urban cooling Model that estimates evapotranspiration directly from land cover.

Within the public health field, the evapotranspiration modeling can function as an example of metric of greenspace exposure that explicitly models greenspace activity rather than abundance to separate different pathways from greenspace to health effect and increase causal understanding of health effects of greenspace. The framework presented here can be applied to various other pathways that link greenspace to health framed as ecosystem services, including particulate matter deposition (Hofman et al., 2013), or noise mitigation (Peng et al., 2014). Each of these services can have several separate independent health effects that each depend on supply, environment, and beneficiaries. Whereas current practice in epidemiology often bundles all potential ecosystem health benefits in a single indicator of vegetation abundance, further application of the ES framework can leverage existing knowledge and expertise of ecosystem functions that could to a more explicit and accurate representation of the health benefits of urban greenspace exposure. The comparison of supply and demand, a very common ES tool, provided a relatively simple method to connect the products from different fields to provide an output that could directly inform urban planning decisions.

As one of the first attempts to explicitly link health related environmental exposure benefits to functions of urban vegetation through an ecosystem services framework, the empirical findings have some limitations. The representation of cooling demand in this paper was based on health risk assessment modeling and showed innovation by modeling heat exposure risk at the residential building level for the entire city of Boston, while incorporating fine scale resolution daily ambient temperature data. Heat vulnerability was calculated by weighting the five vulnerability dimensions equally which may under or overestimate their importance. However, the equation can easily be adapted to a different weighting scheme or incorporate locally important vulnerability dimensions. Moreover, the ACS based vulnerability indicator did not include factors that relate ambient temperature to indoor exposure such as the availability of indoor temperature regulation and insulation. Additionally, we did not include non-residential heat exposures in this analysis. Workplace and transportation heat stress in the US is relatively understudied, but could potentially fuel further health disparities due to differences between outside workplaces and air conditioned spaces (Acharya et al., 2018; Gubernot et al., 2014). Mapping of both demand for benefits and supply of ES, like in this study, often relies on modeling techniques that introduce potential error and bias with every assumption (Schägner et al., 2013). Future studies could build on the framework outlined in this paper to connect the supply of ES-services to spatially explicit health outcomes. However, health outcomes such as heat-related emergency department visits or mortality are very rarely available at fine spatial resolution and when available are at state level (e.g. Kingsley et al., 2016) or zip code level (e.g. Shi et al., 2015).

We used a model that has been validated with field studies and incorporated the most recent insights in urban evapotranspiration modeling (Smith et al., 2021). Ongoing developments outside the realm of environmental health studies can further improve the cooling indicator proposed here by incorporating additional factors that have been proven to affect cooling ecosystem services. These factors include differentiation on types of greenspace such as grass, shrubs, and trees, the differences in service provision of different species (Ballinas and Barradas, 2016), spatial patterns of greenspace (Kong et al., 2014), or the other characteristics of the built environment that can enhance the cooling effect of greenspace such as green roofs, air conditioning, or the albedo effects of different types of pavements (Li et al., 2014; Winbourne et al., 2020). Further climatological modeling and including the effect of shading on ambient temperature could eventually lead to an indicator expressed in the change of ambient temperature in degrees Celsius during heat wave temperatures needed to predict the exact effect of greenspace on heat-related health outcomes.

5. Conclusion

We provided an indicator of exposure to heat reducing ES of urban greenspace by applying a model rooted in ecological theory and based on open data. While the resulting indicator follows a pattern similar to conventional indicators based on vegetation abundance, our modeling efforts highlighted key differences in the importance of urban context for the delivery of cooling ES. In addition, the evapotranspiration modeling applied to this area showed that evapotranspiration increases with rising temperatures, meaning that similar greenspace provides more cooling ES in warmer areas, such as those with higher levels of impervious surface (i.e. UHI). Comparing our indicator of cooling ES supply with an indicator of heat exposure risk serving as a proxy for demand for health benefits of cooling revealed those areas within the city where additional urban vegetation could provide the highest benefits in terms of heat related health outcomes. A focus on ecosystem services instead of vegetation abundance can greatly improve the understanding and application of health benefits of urban greenspace.

References

Acharya, P., Boggess, B., Zhang, K., 2018. Assessing heat stress and health among construction workers in a changing climate: A review. Int. J. Environ. Res. Public Health 15, 247. https://doi.org/10.3390/ijerph15020247

Adams, M.P., Smith, P.L., 2014. A systematic approach to model the influence of the type and density of vegetation cover on urban heat using remote sensing. Landsc. Urban Plan. 132, 47–54. https://doi.org/https://doi.org/10.1016/j.landurbplan.2014.08.008

Aubrecht, C., Özceylan, D., 2013. Identification of heat risk patterns in the U.S. National Capital Region by integrating heat stress and related vulnerability. Environ. Int. 56, 65–77. https://doi.org/10.1016/j.envint.2013.03.005

Ballinas, M., Barradas, V.L., 2016. The Urban Tree as a Tool to Mitigate the Urban Heat Island in Mexico City: A Simple Phenomenological Model. J. Environ. Qual. 45, 157–166. https://doi.org/10.2134/jeq2015.01.0056

Bekkar, B., Pacheco, S., Basu, R., DeNicola, N., 2020. Association of Air Pollution and Heat Exposure With Preterm Birth, Low Birth Weight, and Stillbirth in the US: A Systematic Review. JAMA Netw. Open 3, e208243–e208243. https://doi.org/10.1001/jamanetworkopen.2020.8243

Benjamin, S.G., Weygandt, S.S., Brown, J.M., Hu, M., Alexander, C.R., Smirnova, T.G., Olson, J.B., James, E.P., Dowell, D.C., Grell, G.A., Lin, H., Peckham, S.E., Smith, T.L., Moninger, W.R., Kenyon, J.S., Manikin, G.S., 2016. A North American Hourly Assimilation and Model Forecast Cycle: The Rapid Refresh. Mon. Weather Rev. 144, 1669–1694. https://doi.org/10.1175/MWR-D-15-0242.1

Bishaw, A., 2013. Examining the Effect of Off-Campus College Students on Poverty Rates SEHSD 2013-17. U.S. Census Bur.

Boston Assessing Department, 2019. Massachusetts Property Classification System Occupancy Codes [WWW Document]. URL https://www.cityofboston.gov/images_documents/MA_OCCcodes_tcm3-16189.pdf

Bratman, G.N., Anderson, C.B., Berman, M.G., Cochran, B., de Vries, S., Flanders, J., Folke, C., Frumkin, H., Gross, J.J., Hartig, T., Kahn, P.H., Kuo, M., Lawler, J.J., Levin, P.S., Lindahl, T., Meyer-Lindenberg, A., Mitchell, R., Ouyang, Z., Roe, J., Scarlett, L., Smith, J.R., van den Bosch, M., Wheeler, B.W., White, M.P., Zheng, H., Daily, G.C., 2019. Nature and mental health: An ecosystem service perspective. Sci. Adv. 5, eaax0903. https://doi.org/10.1126/sciadv.aax0903

Burkart, K., Meier, F., Schneider, A., Breitner, S., Canário, P., Alcoforado, M.J., Scherer, D., Endlicher, W., 2016. Modification of heat-related mortality in an elderly urban population by vegetation (Urban green) and proximity to water (Urban blue): Evidence from Lisbon, Portugal. Environ. Health Perspect. 124, 927–934. https://doi.org/10.1289/ehp.1409529

Burkhard, B., Kroll, F., Nedkov, S., Müller, F., 2012. Mapping ecosystem service supply, demand and budgets. Ecol. Indic. 21, 17–29. https://doi.org/10.1016/j.ecolind.2011.06.019

Chiabai, A., Quiroga, S., Martinez-Juarez, P., Higgins, S., Taylor, T., 2018. The nexus between climate change, ecosystem services and human health: Towards a conceptual framework. Sci. Total Environ. 635, 1191–1204. https://doi.org/10.1016/j.scitotenv.2018.03.323

Fisher, B., Turner, K., Zylstra, M., Brouwer, R., De Groot, R., Farber, S., Ferraro, P., Green, R., Hadley, D., Harlow, J., Jefferiss, P., Kirkby, C., Morling, P., Mowatt, S., Naidoo, R., Paavola, J., Strassburg, B., Yu, D., Balmford, A., 2008. Ecosystem services and economic theory: Integration for policy-relevant research. Ecol. Appl. 18, 2050–2067. https://doi.org/10.1890/07-1537.1

Fox, John & Weisberg, S., 2011. An R Companion to Applied Regression, Third. ed. Sage, Thousand Oaks {CA}.

Frumkin, H., Bratman, G.N., Breslow, S.J., Cochran, B., Kahn, P.H., Lawler, J.J., Levin, P.S., Tandon, P.S., Varanasi, U., Wolf, K.L., Wood, S.A., 2017. Nature contact and human health: A research agenda. Environ. Health Perspect. 125, 75001. https://doi.org/10.1289/EHP1663

Gallo, K.P., McNab, A.L., Karl, T.R., Brown, J.F., Hood, J.J., Tarpley, J.D., 1993. The use of a vegetation index for assessment of the urban heat island effect. Int. J. Remote Sens. 14, 2223–2230. https://doi.org/10.1080/01431169308954031

Gorelick, N., Hancher, M., Dixon, M., Ilyushchenko, S., Thau, D., Moore, R., 2017. Google Earth Engine: Planetary-scale geospatial analysis for everyone. Remote Sens. Environ. 202, 18–27. https://doi.org/https://doi.org/10.1016/j.rse.2017.06.031

Gronlund, C.J., Berrocal, V.J., White-Newsome, J.L., Conlon, K.C., O'Neill, M.S., 2015. Vulnerability to extreme heat by socio-demographic characteristics and area green space among the elderly in Michigan, 1990-2007. Environ. Res. 136, 449–461. https://doi.org/10.1016/j.envres.2014.08.042

Gubernot, D.M., Anderson, G.B., Hunting, K.L., 2014. The epidemiology of occupational heat exposure in the United States: a review of the literature and assessment of research needs in a changing climate. Int. J. Biometeorol. 58, 1779–1788. https://doi.org/10.1007/s00484-013-0752-x

Hamel, P., Guerry, A.D., Polasky, S., Han, B., Douglass, J.A., Hamann, M., Janke, B., Kuiper, J.J., Levrel, H., Liu, H., Lonsdorf, E., McDonald, R.I., Nootenboom, C., Ouyang, Z., Remme, R.P., Sharp, R.P., Tardieu, L., Viguié, V., Xu, D., Zheng, H., Daily, G.C., 2021. Mapping the benefits of nature in cities with the InVEST software. npj Urban Sustain. 1, 25. https://doi.org/10.1038/s42949-021-00027-9

Hardiman, B.S., Wang, J.A., Hutyra, L.R., Gately, C.K., Getson, J.M., Friedl, M.A., 2017. Accounting for urban biogenic fluxes in regional carbon budgets. Sci. Total Environ. 592, 366–372. https://doi.org/10.1016/j.scitotenv.2017.03.028

Hess, J.J., Saha, S., Luber, G., 2014. Summertime Acute Heat Illness in U.S. Emergency Departments from 2006 through 2010: Analysis of a Nationally Representative Sample. Environ. Health Perspect. 122, 1209–1215. https://doi.org/10.1289/ehp.1306796

Hofman, J., Stokkaer, I., Snauwaert, L., Samson, R., 2013. Spatial distribution assessment of particulate matter in an urban street canyon using biomagnetic leaf monitoring of tree crown deposited particles. Environ. Pollut. 183, 123–132. https://doi.org/10.1016/j.envpol.2012.09.015

Hu, L., Li, Q., 2020. Greenspace, bluespace, and their interactive influence on urban thermal environments. Environ. Res. Lett. 15, 34041. https://doi.org/10.1088/1748-9326/ab6c30

James, P., Banay, R.F., Hart, J.E., Laden, F., 2015. A Review of the Health Benefits of Greenness. Curr. Epidemiol. Reports 2, 131–142. https://doi.org/10.1007/s40471-015-0043-7

Janhäll, S., 2015. Review on urban vegetation and particle air pollution – Deposition and dispersion. Atmos. Environ. 105, 130–137. https://doi.org/https://doi.org/10.1016/j.atmosenv.2015.01.052

Kent, S.T., McClure, L.A., Zaitchik, B.F., Smith, T.T., Gohlke, J.M., 2014. Heat waves and health outcomes in Alabama (USA): The importance of heat wave definition. Environ. Health Perspect. 122, 151–158. https://doi.org/10.1289/ehp.1307262

Kingsley, S.L., Eliot, M.N., Gold, J., Vanderslice, R.R., Wellenius, G.A., 2016. Current and projected heat-related morbidity and mortality in Rhode Island. Environ. Health Perspect. 124, 460–467. https://doi.org/10.1289/ehp.1408826

Kleerekoper, L., Van Esch, M., Salcedo, T.B., 2012. How to make a city climate-proof, addressing the urban heat island effect. Resour. Conserv. Recycl. 64, 30–38. https://doi.org/10.1016/j.resconrec.2011.06.004

Kong, F., Yin, H., James, P., Hutyra, L.R., He, H.S., 2014. Effects of spatial pattern of greenspace on urban cooling in a large metropolitan area of eastern China. Landsc. Urban Plan. 128, 35–47. https://doi.org/10.1016/j.landurbplan.2014.04.018

Leslie, E., Sugiyama, T., Ierodiaconou, D., Kremer, P., 2010. Perceived and objectively measured greenness of neighbourhoods: Are they measuring the same thing? Landsc. Urban Plan. 95, 28–33. https://doi.org/https://doi.org/10.1016/j.landurbplan.2009.11.002

Li, D., Bou-Zeid, E., Oppenheimer, M., 2014. The effectiveness of cool and green roofs as urban heat island mitigation strategies. Environ. Res. Lett. 9, 55002. https://doi.org/10.1088/1748-9326/9/5/055002

Li, D., Liao, W., Rigden, A.J., Liu, X., Wang, D., Malyshev, S., Shevliakova, E., 2019. Urban heat island: Aerodynamics or imperviousness? Sci. Adv. 5, eaau4299. https://doi.org/10.1126/sciadv.aau4299

Madrigano, J., Ito, K., Johnson, S., Kinney, P.L., Matte, T., 2015. A case-only study of vulnerability to heat wave–related mortality in New York City (2000–2011). Environ. Health Perspect. 123, 672–678. https://doi.org/10.1289/ehp.1408178

Madrigano, J., Lane, K., Petrovic, N., Ahmed, M., Blum, M., Matte, T., 2018. Awareness, risk perception, and protective behaviors for extreme heat and climate change in New York City. Int. J. Environ. Res. Public Health. https://doi.org/10.3390/ijerph15071433

Mahadevan, P., Wofsy, S.C., Matross, D.M., Xiao, X., Dunn, A.L., Lin, J.C., Gerbig, C., Munger, J.W., Chow, V.Y., Gottlieb, E.W., 2008. A satellite-based biosphere parameterization for net ecosystem CO2 exchange: Vegetation Photosynthesis and Respiration Model (VPRM). Global Biogeochem. Cycles 22. https://doi.org/10.1029/2006GB002735

Markevych, I., Schoierer, J., Hartig, T., Chudnovsky, A., Hystad, P., Dzhambov, A.M., de Vries, S., Triguero-Mas, M., Brauer, M., Nieuwenhuijsen, M.J., Lupp, G., Richardson, E.A., Astell-Burt, T., Dimitrova, D., Feng, X., Sadeh, M., Standl, M., Heinrich, J., Fuertes, E., 2017. Exploring pathways linking greenspace to health: Theoretical and methodological guidance. Environ. Res. https://doi.org/10.1016/j.envres.2017.06.028

MassGIS, 2020. Standardized Assessor Parcels.

MassGIS, 2007. MassGIS Data: Impervious Surface 2005. Boston.

Medina-Ramón, M., Schwartz, J., 2007. Temperature, temperature extremes, and mortality: A study of acclimatisation and effect modification in 50 US cities. Occup. Environ. Med. 64, 827–833. https://doi.org/10.1136/oem.2007.033175

Monteith, J.L., 1965. Evaporation and environment., in: Symposia of the Society for Experimental Biology. Cambridge University Press (CUP) Cambridge, pp. 205–234.

Nardone, A., Rudolph, K.E., Morello-Frosch, R., Casey, J.A., 2021. Redlines and greenspace: The relationship between historical redlining and 2010 greenspace across the United States. Environ. Health Perspect. 129, 1–9. https://doi.org/10.1289/EHP7495

NOAA National Centers for Environmental Information, 2017. GOES-R Calibration Working Group and GOES-R Series Program: NOAA GOES-R Series Advanced Baseline Imager (ABI) Level 1b Radiances [WWW Document].

Nouri, H., Beecham, S., Anderson, S., Nagler, P., 2014. High Spatial Resolution WorldView-2 Imagery for Mapping NDVI and Its Relationship to Temporal Urban Landscape Evapotranspiration Factors. Remote Sens. . https://doi.org/10.3390/rs6010580

OpenStreetMap, 2017. Contributers. Planet dump retrieved from https://planet.osm.org.

Peng, J., Bullen, R., Kean, S., 2014. The effects of vegetation on road traffic noise, in: INTERNOISE 2014 - 43rd International Congress on Noise Control Engineering: Improving the World Through Noise Control. Institute of Noise Control Engineering, pp. 600–609.

Phillipson, J., Lowe, P., Bullock, J.M., 2009. Navigating the social sciences: Interdisciplinarity and ecology: Guest Editorial. J. Appl. Ecol. 46, 261–264. https://doi.org/10.1111/j.1365-2664.2009.01625.x

PRISM Climate Group, 2019. PRISM 800m ambient temperatures [WWW Document].

Rankin, B.H., Quane, J.M., 2000. Neighborhood poverty and the social isolation of inner-city African American families. Soc. Forces 79, 139–164. https://doi.org/10.1093/sf/79.1.139

Reid, C.E., O'Neill, M.S., Gronlund, C.J., Brines, S.J., Brown, D.G., Diez-Roux, A. V., Schwartz, J., 2009. Mapping community determinants of heat vulnerability. Environ. Health Perspect. 117, 1730–1736. https://doi.org/10.1289/ehp.0900683

Riley, A.R., 2018. Neighborhood Disadvantage, Residential Segregation, and Beyond—Lessons for Studying Structural Racism and Health. J. Racial Ethn. Heal. Disparities 5, 357–365. https://doi.org/10.1007/s40615-017-0378-5

Sandifer, P.A., Sutton-Grier, A.E., Ward, B.P., 2015. Exploring connections among nature, biodiversity, ecosystem services, and human health and well-being: Opportunities to enhance health and biodiversity conservation. Ecosyst. Serv. 12, 1–15. https://doi.org/10.1016/j.ecoser.2014.12.007

Schägner, J.P., Brander, L., Maes, J., Hartje, V., 2013. Mapping ecosystem services' values: Current practice and future prospects. Ecosyst. Serv. 4, 33–46. https://doi.org/https://doi.org/10.1016/j.ecoser.2013.02.003

Schulp, C.J.E., Lautenbach, S., Verburg, P.H., 2014. Quantifying and mapping ecosystem services: Demand and supply of pollination in the European Union. Ecol. Indic. 36, 131–141. https://doi.org/10.1016/j.ecolind.2013.07.014

Shanahan, D.F., Lin, B.B., Bush, R., Gaston, K.J., Dean, J.H., Barber, E., Fuller, R.A., 2015. Toward improved public health outcomes from urban nature. Am. J. Public Health 105, 470–477. https://doi.org/10.2105/AJPH.2014.302324

Shi, L., Kloog, I., Zanobetti, A., Liu, P., Schwartz, J.D., 2015. Impacts of temperature and its variability on mortality in New England. Nat. Clim. Chang. 5, 988–991. https://doi.org/10.1038/nclimate2704

Smith, I.A., Winbourne, J.B., Tieskens, K.F., Jones, T.S., Bromley, F.L., Li, D., Hutyra, L.R., 2021. A Satellite-Based Model for Estimating Latent Heat Flux From Urban Vegetation. Front. Ecol. Evol. 9. https://doi.org/10.3389/fevo.2021.695995

Spangler, K.R., Wellenius, G.A., 2020. Spatial patterns of recent US summertime heat trends:

Implications for heat sensitivity and health adaptations. Environ. Res. Commun. 2, 035002. https://doi.org/10.1088/2515-7620/ab7abb

Tan, J., Zheng, Y., Song, G., Kalkstein, L.S., Kalkstein, A.J., Tang, X., 2007. Heat wave impacts on mortality in Shanghai, 1998 and 2003. Int. J. Biometeorol. 51, 193–200. https://doi.org/10.1007/s00484-006-0058-3

Tang, J., Bolstad, P. V., Desai, A.R., Martin, J.G., Cook, B.D., Davis, K.J., Carey, E. V., 2008. Ecosystem respiration and its components in an old-growth forest in the Great Lakes region of the United States. Agric. For. Meteorol. 148, 171–185. https://doi.org/10.1016/j.agrformet.2007.08.008

Tieskens, K.F., Schulp, C.J.E., Levers, C., Lieskovský, J., Kuemmerle, T., Plieninger, T., Verburg, P.H., 2017. Characterizing European cultural landscapes: Accounting for structure, management intensity and value of agricultural and forest landscapes. Land use policy 62, 29–39. https://doi.org/10.1016/j.landusepol.2016.12.001

Tomlinson, C.J., Chapman, L., Thornes, J.E., Baker, C.J., 2011. Including the urban heat island in spatial heat health risk assessment strategies: a case study for Birmingham, UK. Int. J. Health Geogr. 10, 42. https://doi.org/10.1186/1476-072X-10-42

Trlica, A., Hutyra, L.R., Schaaf, C.L., Erb, A., Wang, J.A., 2017. Albedo, Land Cover, and Daytime Surface Temperature Variation Across an Urbanized Landscape. Earth's Futur. 5, 1084–1101. https://doi.org/10.1002/2017EF000569

Twohig-Bennett, C., Jones, A., 2018. The health benefits of the great outdoors: A systematic review and meta-analysis of greenspace exposure and health outcomes. Environ. Res. 166, 628–637. https://doi.org/10.1016/j.envres.2018.06.030

Urban Ecology Institute, 2008. State of the Urban Forest: A Summary of the Extent and Condition of Boston's Urban Forest. Newton, MA.

van den Berg, M., Wendel-Vos, W., van Poppel, M., Kemper, H., van Mechelen, W., Maas, J., 2015. Health benefits of green spaces in the living environment: A systematic review of epidemiological studies. Urban For. Urban Green. 14, 806–816. https://doi.org/10.1016/j.ufug.2015.07.008

Wang, J.A., Hutyra, L.R., Li, D., Friedl, M.A., 2017. Gradients of atmospheric temperature and humidity controlled by local urban land-use intensity in Boston. J. Appl. Meteorol. Climatol. 56, 817–831. https://doi.org/10.1175/JAMC-D-16-0325.1

Watson, B.C., Wilson, W.J., 1988. The Truly Disadvantaged: The Inner City, The Underclass, and Public Policy., The Journal of Negro Education. University of Chicago Press. https://doi.org/10.2307/2295455

Winbourne, J.B., Jones, T.S., Garvey, S.M., Harrison, J.L., Wang, L., Li, D., Templer, P.H., Hutyra, L.R., 2020. Tree Transpiration and Urban Temperatures: Current Understanding, Implications, and Future Research Directions. Bioscience 70, 576–588. https://doi.org/10.1093/biosci/biaa055

Xie, Z., 2006. A framework for interpolating the population surface at the residential-housing-unit level. GIScience Remote Sens. 43, 233–251. https://doi.org/10.2747/1548-1603.43.3.233

Yan, C., Guo, Q., Li, H., Li, L., Qiu, G.Y., 2020. Quantifying the cooling effect of urban vegetation by mobile traverse method: A local-scale urban heat island study in a subtropical megacity. Build. Environ. 169, 106541. https://doi.org/10.1016/j.buildenv.2019.106541

Yunusa, I.A.M., Eamus, D., Taylor, D., Whitley, R., Gwenzi, W., Palmer, A.R., Li, Z., 2015. Partitioning of turbulent flux reveals contrasting cooling potential for woody vegetation and grassland during heat waves. Q. J. R. Meteorol. Soc. 141, 2528–2537. https://doi.org/https://doi.org/10.1002/qj.2539

Zardo, L., Geneletti, D., Pérez-Soba, M., Van Eupen, M., 2017. Estimating the cooling capacity of green infrastructures to support urban planning. Ecosyst. Serv. 26, 225–235. https://doi.org/https://doi.org/10.1016/j.ecoser.2017.06.016

Zawadzka, J.E., Harris, J.A., Corstanje, R., 2021. Assessment of heat mitigation capacity of urban greenspaces with the use of InVEST urban cooling model, verified with day-time land surface temperature data. Landsc. Urban Plan. 214, 104163. https://doi.org/https://doi.org/10.1016/j.landurbplan.2021.104163

Zhang, L., Tan, P.Y., Diehl, J.A., 2017. A conceptual framework for studying urban green spaces effects on health. J. Urban Ecol. 3. https://doi.org/10.1093/jue/jux015

Ziter, C.D., Pedersen, E.J., Kucharik, C.J., Turner, M.G., 2019. Scale-dependent interactions between tree canopy cover and impervious surfaces reduce daytime urban heat during summer. Proc. Natl. Acad. Sci. U. S. A. 116, 7575–7580. https://doi.org/10.1073/pnas.1817561116

Mapping the health benefits of greenspace against urban heat exposure through an ecosystem services framework

Supplementary Material

Koen F. Tieskens
Department of Environmental Health, Boston University School of Public Health
Boston, MA, 02118, USA
E-mail: tieskens@bu.edu

Ian A. Smith
Department of Earth and Environment, Boston University
Boston, MA 02215, USA

Raquel B. Jimenez Celsi
Department of Environmental Health, Boston University School of Public Health
Boston, MA, 02118, USA

Lucy R. Hutyra
Department of Earth and Environment, Boston University
Boston, MA 02215, USA

M. Patricia Fabian
Department of Environmental Health, Boston University School of Public Health
Boston, MA, 02118, USA

Keywords: Climate change; Heat exposure; heat vulnerability; urban greenspace; ecosystem services; evapotranspiration modeling

Detailed description of modeling process, terms, and data sources

Step 1) Characterize vegetation activity via estimates of net photosynthesis using the Urban Vegetation Photosynthesis and Respiration model (VPRM)

Here, photosynthesis is defined as the gross ecosystem exchange (GEE) of carbon dioxide (CO_2) between the biosphere and the atmosphere. Estimates are derived at an hourly temporal resolution and 30m x 30m spatial resolution. GEE (μmol CO_2 m^2 s^{-1}) is estimated as a function of incoming photosynthetically active radiation (PAR) using the methods, equations, and parameters derived in Mahadevan et al. (2008) and Hardiman et al. (2017) as:

$$GEE = \delta \cdot T_{scale} \cdot P_{scale} \cdot W_{scale} \cdot EVI \cdot \frac{1}{1 + {PAR}/{PAR_0}} \cdot PAR$$

where T_{scale}, P_{scale}, and W_{scale} are dimensionless scaling terms ranging from zero to one describing the influence of air temperature, phenology, and moisture on photosynthesis. *PAR* is photosynthetically active radiation (μmol m^2 s^{-1}). δ and and PAR_0 are plant functional type-specific parameters describing the light-use efficiency (μmol CO_2 μmol PAR^{-1}) and half-saturation value (μmol m^2 s^{-1}) of *GEE* as a function of *PAR*. *EVI* is the Enhanced Vegetation Index.

T_{scale} captures the impact of air temperature on vegetation activity and scales estimates of *GEE* as:

$$T_{scale} = \frac{(T - T_{min})(T - T_{max})}{(T - T_{min})(T - T_{max}) - (T - T_{opt})^2}$$

Where T is the air temperature, T_{min} is the minimum temperature for photosynthesis, T_{max} is the maximum temperature for photosynthesis, and T_{opt} is the optimal temperature for photosynthesis. To account for persistent stomatal activity in vegetation in Boston at the heatwave temperatures experienced during the modeling period (Winbourne et al. 2020), T_{scale} was set to 1 for any temperature greater than 20°C. For temperatures less than 20°C, T_{min} was set to 0°C, T_{opt} was set to 20°C, and T_{max} was set to 40°C (default optimized parameters for deciduous broadleaf trees; Mahadevan et al. 2008).

P_{scale} captures the impact of leaf age on vegetation activity. In this exercise, the modeling period occurred after full leaf expansion and prior to the onset of senescence, therefore, P_{scale} was set to 1.

W_{scale} captures the impact of moisture availability on vegetation activity and scales *GEE* as:

$$W_{scale} = \frac{1 + LSWI}{1 + LSWI_{max}}$$

Where *LSWI* is the Land Surface Water Index and $LSWI_{max}$ is the maximum *LSWI* observed for a given pixel during the growing season. *LSWI* has been proven to effectively monitor vegetation water content (Gu et al. 2008, Xiao et al. 2005, and Maki et al. 2004) and is sensitive to decreases in moisture availability in ecosystems that senesce during drought periods, such as those in Boston, MA.

Estimates of ecosystem respiration are required to determine net canopy assimilation rates of CO_2 (A_n; μmol CO_2 m^2 s^{-1}) and is estimated as:

$$R_{eco} = T \cdot \alpha + \beta$$

Where *T* is the air temperature (°C), α is the sensitivity of R_{eco} to *T*, and β is the minimum value that R_{eco} can take on (μmol CO_2 m^{-2} s^{-1}). In this application, α is set to 0.127 and β is set to 0.25 (Mahadevan et al. 2008). Leaf respiration typically accounts for 8-12% of ecosystem respiration (Tang et al. 2008) and is approximated to be 10% of R_{eco}. Therefore, net photosynthesis of the canopy is estimated as:

$$A_n = GEE - 0.1 \cdot R_{eco}$$

Driver data for the VPRM come from a range of remote-sensing and modeling products. *LSWI* and *EVI* are retrieved every eight days over the course of the year from the Landsat 7 and Landsat 8 Tier 1 Surface Reflectance products and are calculated as:

$$EVI = 2.5(\frac{(NIR - R)}{(NIR + 6R - 7.5B + 1)})$$

where *NIR, R,* and *B* correspond to the surface reflectance measured from the near-infrared, red, and blue bands on the specific Landsat sensor, and:

$$LSWI = \frac{(NIR - SWIR)}{(NIR + SWIR)}$$

where *SWIR* corresponds to the surface reflectance measured from the shortwave infrared band on the specific Landsat sensor. Daily *EVI* and *LSWI* are estimated via interpolation using a spline function and the surface reflectance images.

PAR data come from measurements of incoming shortwave radiation (SW; W m^{-2}) from the Geostationary Operational Environmental Satellite (GOES) 16 at a spatial resolution of 0.05° x 0.05° and hourly temporal resolution. *PAR* (μmol m^2 s^{-1}) is approximated to be SW / 0.505. Air temperature data come from the Rapid Refresh analysis product at a spatial resolution of 13km x 13km and temporal resolution of one hour. For 30m x 30m pixels with impervious surface area greater than 0, air temperature is adjusted as a linear function of impervious surface area and hour of year using the coefficients derived in Wang et al. (2017) and methods described in Hardiman et al. (2017).

Step 2) Estimate surface conductance of water vapor as a function of net photosynthesis

Surface conductance at 30m x 30m spatial resolution and hourly temporal resolution is estimated using the Medlyn stomatal conductance model (2011) as:

$$g_s = g_0 + 1.6 \cdot \left(1 + \frac{g_1}{D}\right) \cdot \frac{A_n}{c_s / P_{atm}} \qquad (6)$$

where g_s is the surface conductance (μmol H_2O m^{-2} s^{-1}), g_0 is the minimum surface conductance (100 μmol H_2O m^{-2} s^{-1}), g_1 is a unitless plant functional type dependent parameter, D is the vapor pressure deficit (kPa), A_n is net photosynthesis (μmol CO_2 m^{-2} s^{-1}), c_s is the partial pressure of CO_2 (40.53 Pa), and P_{atm} is the atmospheric pressure (101325 Pa). In this analysis, the plant functional type parameters for temperature deciduous broadleaf trees were selected. P_{atm} and c_s are held constant due to little sensitivity of model outputs to variations in their values. D is calculated from RAP temperature and relative humidity at a height of 2m aboveground, where values are adjusted to account for urban heat and dry islands as a linear function of impervious surface area and hour of year using the coefficients derived in Wang et al. (2017).

Step 3) Input surface conductance estimates into Penman-Monteith equation to estimate latent heat flux

Latent heat flux (λE; W m^{-2}) is estimated at 30m x 30m spatial resolution and hourly temporal resolution is estimated using the Penman-Monteith model of evapotranspiration (1965) as:

$$\lambda E = \frac{\Delta(R_n - G) + \rho_a c_p (D) g_a}{\Delta + \gamma\left(1 + g_a / g_s\right)}$$

where λ is the latent heat of vaporization of H_2O (2260 J g^{-1}), E is the mass H_2O evaporation rate (g s^{-1} m^{-2}), Δ describes the rate of change of saturation specific humidity with air temperature (Pa K^{-1}), R_n is the net radiation balance of the surface (W m^{-2}), G is the ground heat flux (W m^{-2}), ρ_a is the dry air density (1.275 kg m^{-3}), c_p is the specific heat capacity of air (1005 J kg^{-1} K^{-1}), D is the vapor pressure deficit (Pa), g_a is the atmospheric conductance (m s^{-1}), g_s is the surface conductance (m s^{-1}), and γ is the psychrometric constant (66 Pa K^{-1}).

Δ is calculated following the methods described in Allen et al. (1998) as:

$$\Delta = \frac{4098\left[0.6108\exp\left(\frac{17.27T}{T+237.3}\right)\right]}{(T+237.3)^2}$$

Where *T* is the impervious surface area adjusted air temperature from the RAP product. R_n is estimated to be:

$$R_n = (1-\ \alpha)K\downarrow + L\downarrow\ - (\varepsilon\sigma T_s^4 + (1-\ \varepsilon)L\downarrow)$$

Where α is the 30m x 30m albedo (Trlica et al. 2017), $K\downarrow$ is incoming shortwave radiation (W m^{-2}; acquired from GOES-16), $L\downarrow$ is incoming longwave radiation (W m^{-2}; acquired from GOES-16), ε is the surface emissivity (Estimated to be 0.95 in urban areas; Oke 2017), σ is the Stefan-Boltzman constant (5.67×10^{-8} W m^{-2} K^{-4}), and T_s is the surface temperature (K; acquired from RAP temperature at ground surface). *G* is approximated as 10% of R_n. The dry air density (ρ_a) and specific heat capacity of air (c_p) are held constant as the model outputs show little sensitivity to variations in their values. The aerodynamic conductance (g_a) is estimated to be 0.033 m s^{-1} as the Penman-Monteith equation is not sensitive to variation in aerodynamic conductance in the range of 0.010 – 0.033 m s^{-1} and typical measured values in cities have been found to fall within this range (Ballinas et al. 2016, Chen et al. 2011, Grimmond & Oke 1999).

References

Allen R, Pereira L, Smith M. 1998. Crop Evapotranspiration. Guidelines for Computing Crop Water Requirements. In FAO Irrigation and Drainage Paper (Vol. 56).

Ballinas M, Barradas VL. 2016. The Urban Tree as a Tool to Mitigate the Urban Heat Island in Mexico City: A Simple Phenomenological Model. J Environ Qual 45:157–166; doi:10.2134/jeq2015.01.0056.

Chen L, Zhang Z, Li Z, Tang J, Caldwell P, Zhang W. 2011. Biophysical control of whole tree transpiration under an urban environment in Northern China. Journal of Hydrology 402:388-400. doi:10.1016/j.jhydrol.2011.03.034

Grimmond CS, Oke TR. 1999. Aerodynamic Properties of Urban Areas Derived from Analysis of Surface Form. Journal of Applied Meteorology 38:1262-1292. doi:10.1175/1520-0450(1999)038

Gu Y, Hunt E, Wardlow B, Basara JB, Brown JF, Verdin JP. 2008. Evaluation of MODIS NDVI and NDWI for Vegetation Drought Monitoring Using Oklahoma Mesonet Soil Moisture Data. Geophysical Research Letters 35:L22401.

Hardiman BS, Wang JA, Hutyra LR, Gately CK, Getson JM, Friedl MA. 2017. Accounting for urban biogenic fluxes in regional carbon budgets. Sci Total Environ 592:366–372; doi:10.1016/j.scitotenv.2017.03.028.

Mahadevan P, Wofsy SC, Matross DM, Xiao X, Dunn AL, Lin JC, et al. 2008. A satellite-based biosphere parameterization for net ecosystem CO2 exchange: Vegetation Photosynthesis and Respiration Model (VPRM). Global Biogeochem Cycles 22; doi:10.1029/2006GB002735.

Maki M, Ishiahra M, Tamura M. 2004. Estimation of Leaf Water Status to Monitor the Risk of Forest Fires by Using Remotely Sensed Imagery. Remote Sensing of Environment 90: 441−450.

Medlyn BE, Duursma RA, Eamus D, Ellsworth DS, Prentice IC, Barton CVM, Crous KY, Angelis PD, Freeman M, Wingate L. 2011. Reconciling the optimal and empirical approaches to modelling stomatal conductance. Global Change Biology, 17: 2134–2144. doi:10.1111/j.1365-2486.2010.02375.x

Monteith JL. 1965. Evaporation and environment. Symp Soc Exp Biol 19: 205–234.

Oke, T., Mills, G., Christen, A., & Voogt, J. (2017). Urban Climates. Cambridge: Cambridge University

Press. doi: 10.1017/9781139016476

Tang J, Bolstad P V., Desai AR, Martin JG, Cook BD, Davis KJ, et al. 2008. Ecosystem respiration and its components in an old-growth forest in the Great Lakes region of the United States. Agric For Meteorol 148:171–185; doi:10.1016/j.agrformet.2007.08.008.

Trlica A, Hutyra LR, Schaaf CL, Erb A, Wang JA. 2017. Albedo, Land Cover, and Daytime Surface Temperature Variation Across an Urbanized Landscape. Earth's Futur 5:1084–1101; doi:10.1002/2017EF000569.

Urban Ecology Institute. State of the Urban Forest: A Summary of the Extent and Condition of Boston's Urban Forest. 2008.

Wang JA, Hutyra LR, Li D, Friedl MA. 2017. Gradients of atmospheric temperature and humidity controlled by local urban land-use intensity in Boston. J Appl Meteorol Climatol 56:817–831; doi:10.1175/JAMC-D-16-0325.1.

Winbourne JB, Jones TS, Garvey SM, Harrison JL, Wang L, Li D, et al. 2020. Tree Transpiration and Urban Temperatures: Current Understanding, Implications, and Future Research Directions. Bioscience

Xiao X, Boles S., Liu J., Zhuang D., Frolking S., Li C., Salas W., Moore III B. 2005. Mapping Paddy Rice Agriculture in Southern China Using Multi-Temporal MODIS Images. Remote Sensing of Environment 95: 480–492.